ACS Sustainable Chemistry & Engineering

Research Article

Cite This: ACS Sustainable Chem. Eng. 2019, 7, 13379−13390

pubs.acs.org/journal/ascecg

Free-Standing Graphene Oxide−Chitin Nanocrystal Composite Membrane for Dye Adsorption and Oil/Water Separation

Xianfeng Ou, Xiaohan Yang, Jingqi Zheng, and Mingxian Liu*

Department of Materials Science and Engineering, Jinan University, 601 Huangpu Avenue West, Tianhe District, Guangzhou 510632, China

Supporting Information

ABSTRACT: Chitin nanocrystals modified by dopamine (D-ChNCs)/graphene oxide (GO) composite membranes were successfully prepared with the assistance of vacuum filtration. D-ChNCs/GO was analyzed by Fourier transform infrared spectroscopy (FTIR), X-ray diffraction (XRD), thermogravimetric analysis (TGA), X-ray photoelectron spectroscopy (XPS), and transmission electron microscopy (TEM). Atomic force microscopy (AFM) and scanning electron microscopy (SEM) were used to characterize the surface morphology of the membrane. The hydrophilicity of membrane is dependent on the content of the hydrophilic D-ChNCs, which shows a sharp increase of pure water flux from 8.8 of pure GO to 135.6 $L \cdot m^{-2} \cdot h^{-1}$. The rejection ratio of methylene blue (MB) and Congo red (CR) is as high as 99.3 and 98.3%, respectively. In addition, the oil rejection ratio of the membrane is above 97.5%, exhibiting good oleophobicity. The recycle experiment also demonstrates acceptable recyclability and proper regeneration for practical application. In total, D-ChNCs/GO composite membranes with excellent hydrophilicity, good oleophobicity, and anti-dye and anti-oil fouling have great potential in wastewater treatment.

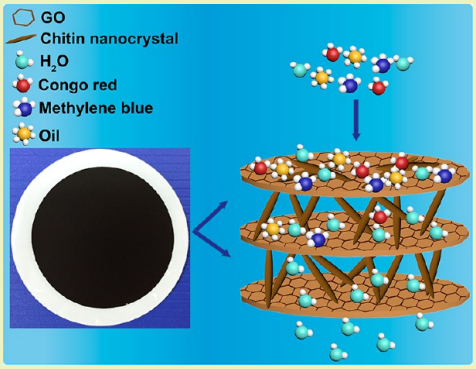

KEYWORDS: *Graphene oxide, Chitin nanocrystals, Dopamine, Free-standing membrane, Wastewater treatment*

INTRODUCTION

With the development of global industry, water pollution has become one of the serious problems over the world in recent decades. Polluted water usually includes various dyes, insoluble oil, and metal ions, which damage drinking water and public health.[1] Nanoadsorbents have been widely exploited as wastewater treatment materials, such as carbon nanotubes,[2] cellulose nanocrystals,[3] halloysite nanotubes,[4] and graphene oxide nanosheets.[5] Due to their nanoscale, high specific area surface, active surface, and good mechanical property, nanoadsorbents could selectively separate organic dyes, metal ions, and oil from water.[2]

Graphene oxide (GO) nanosheets are composed of two-dimensional sp^2-hybridized carbon, with plentiful functional oxygen groups (hydroxyl, epoxy, carbonyl, and carboxyl) on their surfaces.[6] GO has aroused great interests in recent years for its excellent properties of large specific surface area, easily modification, high adsorption performance, good water-dispersion ability, and biocompatibility.[7,8] GO has been extensively used in chemical sensors,[9] energy storage and conversion,[10] and biosensors.[11] In recent years, GO-based membranes have been exploited as adsorbents of dyes, metal ions, and oil, which can be used in the applications of water purification and wastewater treatment systems.[12,13] However, GO prepared by the Hummers method exhibits a narrow layer spacing of 0.68 nm between adjacent GO nanosheets,[14] which hinders rapid and selective permeation of water and other ions. Intercalating nanoscaled guest into GO nanosheets is expected to be the main choice to increase the layer spacing. For instance, GO nanosheets were self-assembled with palygorskite nanorods via vacuum-assisted filtration, which enlarged transfer channels of lamellated GO nanosheets, exhibiting a superior permeated flux of 1867 $L \cdot m^{-2} \cdot h^{-1}$.[15] Halloysite nanotubes modified by dopamine were also intercalated into layered GO sheets, resulting in a high water permeability (218 $L \cdot m^{-2} \cdot h^{-1}$), good dye rejection, and excellent anti-oil-fouling property.[16] GO nanofiltration membrane intercalated by carbon nanotubes showed a high water flux (56.5 $L \cdot m^{-2} \cdot h^{-1}$), good separation efficiency of organic dyes and salt ions, and excellent antifouling performance for sodium alginate and humic acid.[17]

Chitin, the most abundant polysaccharide in nature next to cellulose, can be easily extracted from shellfish, fungi, and insects.[18] Chitin nanocrystals (ChNCs) obtained by removing the amorphous domains of chitin, have attracted enormous interests because of their unique needlelike morphology, high aspect ratios, high specific surface area, high longitudinal moduli and plenty of surface functional groups.[19] ChNCs have been extensively studied as a nanofiller to reinforce polymer matrixes in the applications of tissue engineering, wound-

Received: May 10, 2019
Revised: June 29, 2019
Published: July 9, 2019

DOI: 10.1021/acssuschemeng.9b02619
ACS Sustainable Chem. Eng. 2019, 7, 13379−13390

dressing membrane, sensors, and packing.[20,21] To the best of our knowledge, no literature has stressed the potential of ChNCs for selective permeation in wastewater treatment. However, cellulose nanocrystals have been reported in the field of wastewater separation. For example, cellulose nanocrystals/palygorskite nanorod membranes were fabricated for multifunctional oil/water emulsion separation, showing a high water flux, good oil rejection, and excellent reusability.[22] Assembled by vacuum filtration, fibrous cellulose nanocrystal membranes exhibited good properties of superhydrophilicity and underwater superoleophobicity.[23] Attributed to high porosity of 96.3−97.2%, cellulose nanocrystal aerogel was also used as oil/water separation materials, exhibiting absorption capacity of water, ethanol, toluene, and dodecane.[24] Therefore, ChNCs are expected with great potential as nanomaterials for wastewater separation.

Synergistically intercalating needlelike ChNCs into GO laminate structures is an effective strategy as a multifunctional organic dyes adsorbent and oil/water separation. First, the spacing of adjacent GO nanosheets could be enlarged upon the intercalation of ChNCs, which results in the formation of nanochannels for water molecules. Second, attributed to a large number of hydrophilic groups on its surface such as hydroxyl, *N*-acetyl, and amino groups, ChNCs could greatly enhance the hydrophilicity of GO composite.[19] Constructing a hierarchical nanostructure with ChNCs and interlayered GO nanosheets is beneficial to form a passageway to separate water molecules and oil.

In this work, ChNCs were first modified by dopamine to enhance its hydrophilicity. ChNCs modified by dopamine (D-ChNCs) were then intercalated into stacked GO nanosheets via vacuum-assisted filtration self-assembly. A series of characterizations of the composite membranes were carried out to analyze the chemical composition, crystal structure, thermal behavior, and morphologies. The water flux and hydrophilicity of GO composite membranes were tailored by the content of D-ChNCs. The separation ability and antifouling property were further evaluated against methylene blue (MB), Congo red (CR), and different oil/water mixtures. The free-standing D-ChNCs/GO composite membrane exhibits good wettability, oleophobicity, high separation efficiency, and good reusability, showing potential applications in dye-polluted oil/water separation.

EXPERIMENTAL SECTION

Chemicals and Materials. Chitin was obtained from Wuhan Hezhong Biochemical Manufacturing Co., Ltd., China. Dopamine hydrochloride (purity of ∼98%) was supplied by Shanghai Aladdin Co., Ltd., China. Tris-HCl buffer solution was purchased from Beijing Solarbio Science & Technology Co., Ltd., China. Graphene oxide (GO) dispersion (10 mg/mL) was provided by Knano Graphene Technology Co., Ltd., China. Cellulose acetate membranes (CAMs) (with a diameter of 4 cm and average pore size of 0.45 μm) were provided by Branch billion Lung Experimental Equipment Co. Ltd., Tianjin, China. Molecular weight cutoff (MWCO) of CAM was 19 000 Da. Water was purified by a Milli-Q water system (resistivity >18.2 MΩ/cm). All other chemicals were analytical-grade.

Preparation of ChNCs and ChNCs Modified by Dopamine (D-ChNCs). ChNCs were prepared from chitin according to a typical acid hydrolysis method.[25] First, 20 g of chitin and 3 mol/L HCl were heated at 104 °C for 3 h under vigorously stirring. Then, the mixture was collected and washed by centrifugation with ultrapure water, and this process was repeated three times. Finally, the suspension was dialyzed in flowing water and ChNC powder was collected by a SCIENTZ-12ND vacuum freeze-dryer (Ningbo Scientz Biotechnology Co., Ltd., China). D-ChNCs were prepared by a following synthesis process, and 100 mg of obtained ChNCs and 200 mg of dopamine hydrochloride were dispersed into 20 mL of Tris-HCl buffer solution by an ultrasonic cell disruptor (JY99-IIDN, Ningbo Scientz Biotechnology Co., Ltd., China) for 10 min. The pH of mixture was adjusted to 8.5 and then magnetically stirred for 12 h. Finally, the mixture was collected and washed by centrifugation with ultrapure water, and this process was repeated three times. D-ChNC precipitates were then diluted to 50 mL of suspension.

Preparation of D-ChNCs/GO Composite Membranes. As-prepared D-ChNC suspension (1.8 mg/mL, 10 mL) was homogeneously diluted to 200 mL by ultrasonication. Uniform GO dispersion (0.1 mg/mL) was also prepared by ultrasound. GO dispersion (10 mL) was mixed with different D-ChNC suspensions (10, 20, 30, and 40 mL). The different contents of D-ChNCs and GO mixture were then filtered on the CAMs by vacuum filtration (ILMVAC GmbH, Germany) (2 mbar). M0, M1, M2, M3, and M4 are represented as pure GO suspensions and different volume ratios of GO and D-ChNC solution (1:1, 1:2, 1:3, and 1:4). The synthesis process of D-ChNCs and D-ChNCs/GO composite membranes is schematically illustrated in Figure 1.

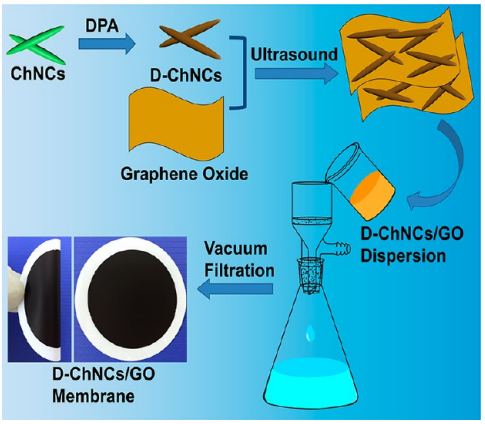

Figure 1. Schematic showing the preparation process of D-ChNCs and D-ChNCs/GO composite membranes.

Preparation of the Oil/Water Emulsions. Sunflower seed oil/water emulsion (10 g/L) was stirred with 0.2 g/L sodium dodecyl sulfate (emulsifier) for 6 h. Similarly, vacuum pump oil/water and dimethyl silicone oil/water emulsion were prepared. The oil concentration was measured by an ultraviolet spectrophotometer based on Beer's law (a substance's concentration and its absorbance were directly proportional).

Characterization. The X-ray diffraction (XRD) patterns of CAM, ChNCs, D-ChNCs, GO, and D-ChNCs/GO were obtained on an X-ray diffractometer (MiniFlex-600, Rigaku Corporation, Japan) with a scanning speed of 10°/min ranging from 3 to 60°. Fourier transform infrared spectroscopy (FTIR) spectra of CAM, ChNCs, D-ChNCs, GO, and different contents of D-ChNCs/GO composite membranes were characterized by a Thermo FTIR instrument (Nicolet iS50, Thermo Fisher Scientific Ltd., USA) from 4000 to 500 cm^{-1}. The thermal stabilities of GO, ChNCs, D-ChNCs, and D-ChNCs/GO were analyzed by a TGA instrument (Mettler Toledo, Switzerland) from 50 to 500 °C at a heating rate of 10 °C/min under a N_2 atmosphere. The elemental composition and the atoms of C, O, and N of pure GO membrane and D-ChNCs/GO composite membrane were detected with an X-ray photoelectron spectroscopy (XPS) instrument (ESCALAB250Xi, Thermo Fisher Scientific Ltd., USA). The morphology of ChNCs, D-ChNCs, and D-ChNCs/GO was analyzed by a transmission electron microscopy (TEM) (JEM-2100F, JEOL Ltd., Japan). The concentration of ChNCs, D-ChNCs, and D-ChNCs/GO for TEM test was 0.05, 0.01, and 0.01 wt %, respectively. The surface morphology of pure GO membrane,composite membranes, CAM, and elemental mapping of C, O, and N in the

DOI: 10.1021/acssuschemeng.9b02619
ACS Sustainable Chem. Eng. 2019, 7, 13379−13390

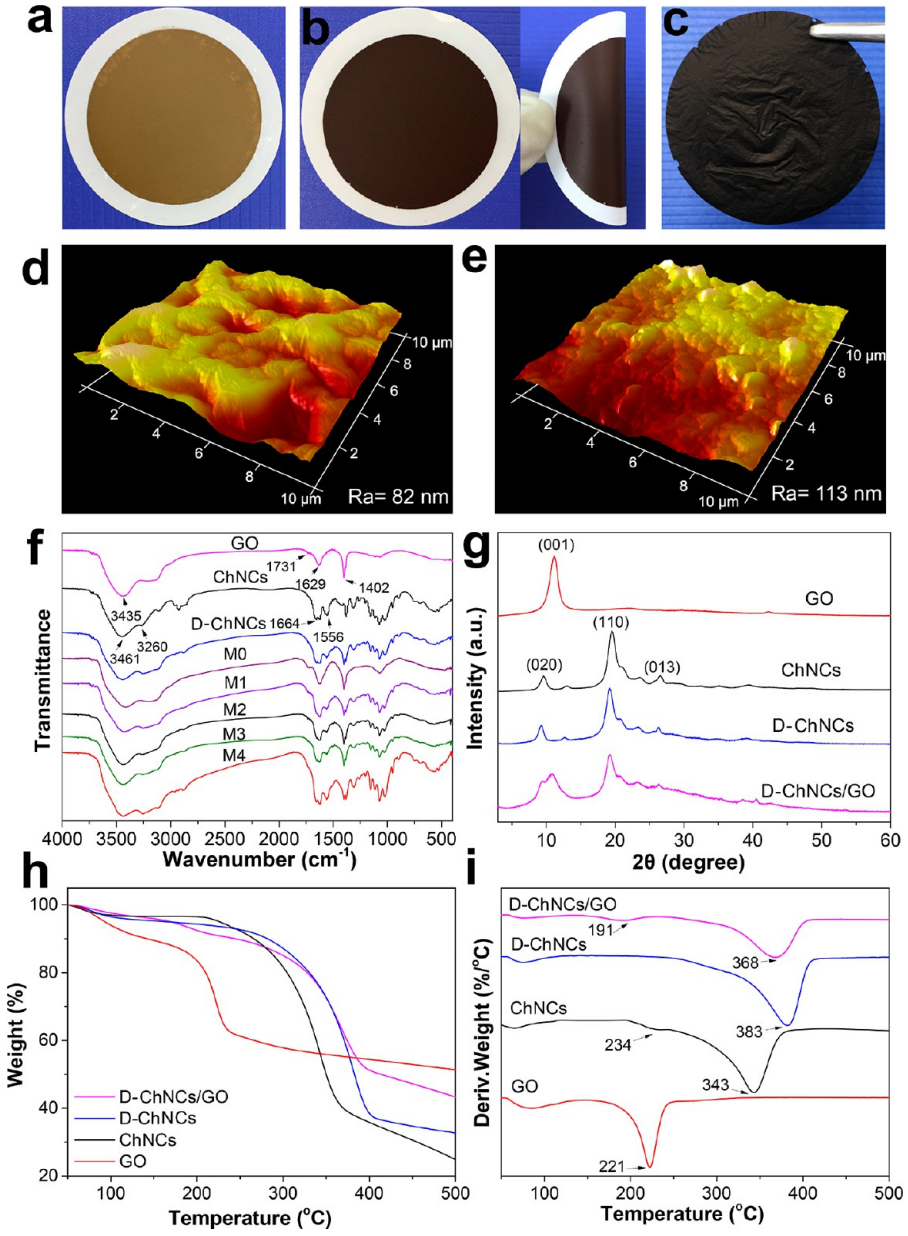

Figure 2. Appearance of M0 (a) and M3 (b and c); 3D AFM images of M0 (d) and M3 (e); FTIR spectra (f), XRD patterns (g), TGA (h), and differential thermogravimetry (i) of GO, ChNCs, D-ChNCs, and D-ChNCs/GO composite.

D-ChNCs/GO composite membrane were conducted by a scanning electron microscopy (SEM) (Ultra 55 SEM instrument, ZEISS, Germany) at a voltage of 5 kV. Atomic force microscopy (AFM) (Bioscope Catylyst Nanoscope-V, Broker Instruments Ltd., USA) was used to test the surface roughnesses of membranes with a scanning area of 10 μm × 10 μm. The zeta potentials of CAM, GO membrane, and M4 were characterized by a solid surface zeta potential analyzer (SurPASS 3, Austria).

Water Contact Angle Measurement and Pure Water Flux of Composite Membranes. The surface hydrophilicity and wettability of the composite membranes were determined by a contact angle instrument (DSA100, Kruss Ltd., Germany) with a liquid droplet volume of 5.0 μL at room temperature. The pure water flux ($L \cdot m^{-2} \cdot h^{-1}$) of composite membranes was determined by the following formula

$$\text{pure water flux} = \frac{V}{A \times t} \quad (1)$$

where V, A, and t, are the volume of permeated water (L), effective membrane area (m^2), and permeation time (h), respectively. All the measurements were reliably obtained by testing at least three samples.

Dye Separation Performance of Composite Membranes. First, 20 mg/L MB and 20 mg/L CR were permeated by vacuum filtration on M0, M1, M2, M3, and M4, respectively. The permeation times of dye solution were recorded. Meanwhile, dye loadings with 10 g/L NaCl solution were also filtered on M4. The concentration of feed solution and permeation solution was determined using an ultraviolet spectrophotometer (UV-2550, Shimadzu Instrument Ltd., China). The maximum absorbance wavelengths of MB and CR were at 664 and 488 nm, respectively. The rejection ratio of MB and CR was calculated using the formula

$$\text{rejection ratio} = \left(1 - \frac{C_p}{C_f}\right) \times 100\% \quad (2)$$

where C_f and C_p are the concentration of feed solution and permeation solution (mg/L), respectively.

DOI: 10.1021/acssuschemeng.9b02619
ACS Sustainable Chem. Eng. 2019, 7, 13379−13390

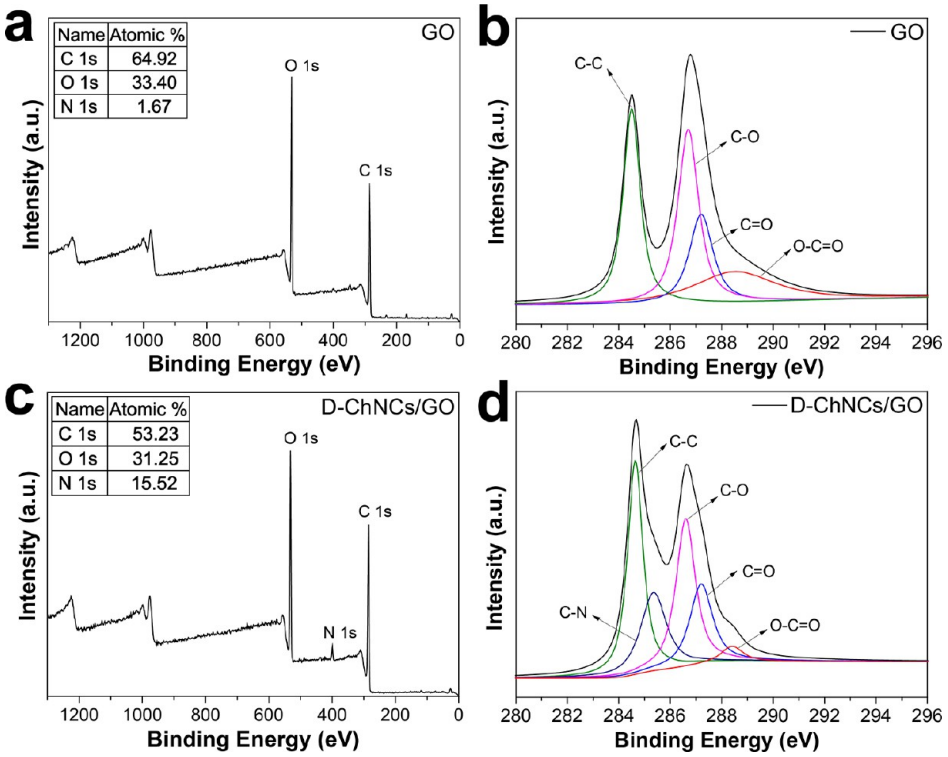

Figure 3. XPS survey spectra for GO (a), D-ChNCs/GO (c); C 1s spectra for GO (b), D-ChNCs/GO (d).

Underwater-Oil Contact Angle Measurement. Underwater-oil contact angle of composite membrane was measured by the contact angle instrument (DSA100, Kruss Ltd., Germany) with a needle diameter of 0.5 mm. The measurements were reliably obtained by testing at least three parallel samples.

Oil/Water Separation Performance of Composite Membranes. As-prepared sunflower seed oil-, dimethyl silicone oil-, and vacuum pump oil-in-water emulsion (10 g/L) were filtered on different membranes. The concentration of feed solution and permeation solution was determined by an ultraviolet spectrophotometer.

Reusable and Antifouling Property Evaluation. Antifouling experiment was used to evaluate anti-oil/-dye fouling of membrane and recycling property. Then, 10 mL of feed solution was filtrated on the composite membrane. The dye and oil droplets were washed by ethanol solution and ultrapure water for 10 min, respectively. Five rounds antifouling test were carried out continuously.

RESULTS AND DISCUSSION

Characterization of Composite Membrane. The GO membrane and D-ChNCs/GO membrane both show a smooth and flat appearance in Figure 2a,b, which is due to the GO sheet being stacked layer-by-layer during vacuum filtration self-assembly. The composite membrane is thin and absolutely free-standing in a dry state (Figure 2c). The stability and the mechanical properties of the membrane are significant for their practical application. However, the mechanical experiment of the D-ChNCs/GO composite membrane is difficult to test due to their fragility. The 3D surface morphology of membranes was analyzed using AFM in Figure 2d,e. The 3D image of pure GO membrane exhibits nanoscale wrinkles like low-lying up and down hills, while the surface morphology of D-ChNCs/GO composite membrane displays numerous sharp mountain peaks. As needlelike D-ChNCs are intercalated into hierarchical GO nanosheets, the surface roughness of composite membrane obviously increases compared to M0. The enhancement of membrane roughness could enlarge the surface area of membrane, which results in more oil droplets absorbed on the membrane surface.[26] Moreover, the larger surface roughness could improve underwater oleophobicity of membrane interfaces.[15] The result is also confirmed in the following oleophobicity test. The zeta potential of CAM and GO membrane is −29.92 and −59.19 mV, while the zeta potential of D-ChNCs/GO membrane is −14.97 mV due to the introduction of positively charged ChNCs. The FTIR spectra of GO, ChNCs, D-ChNCs, and D-ChNCs/GO with different contents of D-ChNCs are shown in Figure 2f. The characteristic peaks of GO at 3435, 1731, 1629, and 1402 cm^{-1} are assigned to O−H stretching vibration, C═O stretching vibration, C═C stretching of the phenol ring, and carboxyl C−O, respectively.[27,28] For unmodified ChNCs, the adsorption bands are at 3461 cm^{-1} (O−H stretching), 3260 cm^{-1} (N−H stretching), 1664 cm^{-1} (amide I), and 1556 cm^{-1} (amide II), respectively.[29] D-ChNCs exhibit a broader adsorption peak at around 3400 and 3260 cm^{-1} related to the stretching vibrations of O−H and N−H, suggesting the enhancement of surface hydrophilicity by the modification of polydopamine (PDA) layers that were polymerized by dopamine with catechol and amine groups at pH 8.5.[30] The composites show an increased adsorption peak at 3400 cm^{-1} due to the addition of hydrophilic D-ChNCs. In addition, a sharp peak emerges at 1402 cm^{-1} of carboxyl C−O for GO nanosheets, which demonstrates that composites are composed of both D-ChNCs and GO nanosheets. Figure 2g shows the XRD patterns of GO, ChNCs, D-ChNCs, and D-ChNCs/GO. The diffraction peak of GO appears at 2θ = 11.3° which is associated with the characteristic peak (001 plane) of interlayer GO nanosheets.[31] The diffraction peaks of ChNCs appear at 9.6° (020 plane), 19.6° (110 plane), and 26.7° (013 plane).[32] The diffraction peaks of D-ChNCs are similar to those in

DOI: 10.1021/acssuschemeng.9b02619
ACS Sustainable Chem. Eng. 2019, 7, 13379−13390

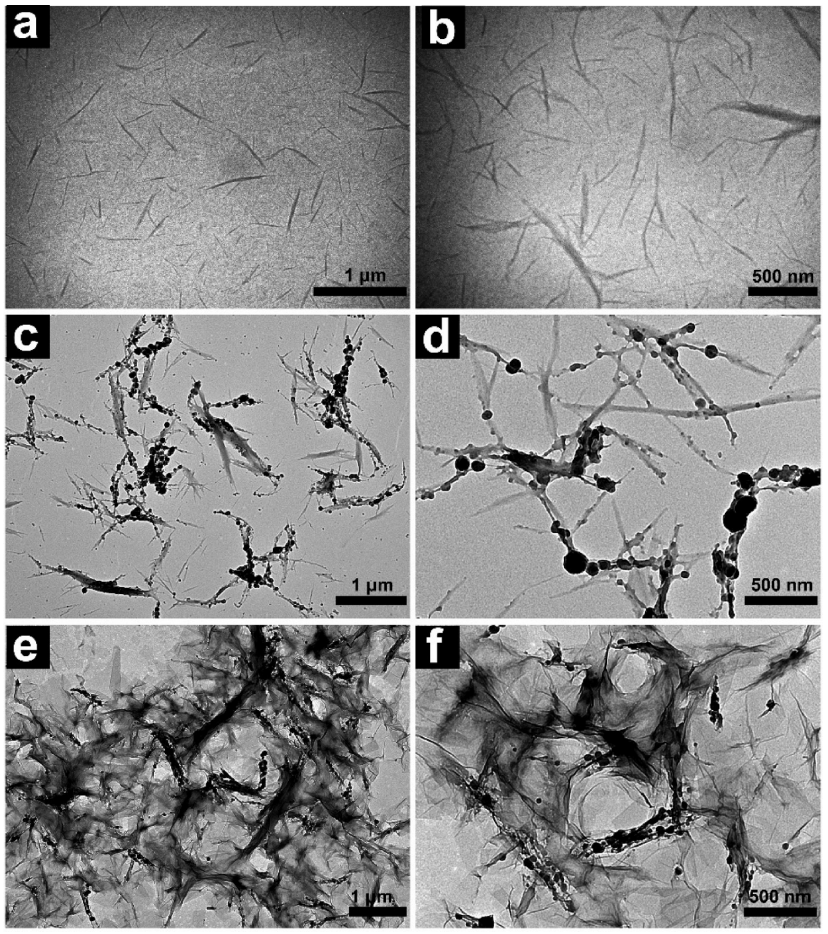

Figure 4. TEM images of ChNCs (a, b), D-ChNCs (c, d), and D-ChNCs/GO (e, f).

ChNC pattern, suggesting that PDA does not change crystalline structure of ChNCs. D-ChNCs/GO shows broader diffraction peaks at 2θ = 9−13° and 15−45°, which are attributed to the presence of D-ChNCs and GO. D-ChNCs are considered to be intercalated into the layered GO nanosheets. Figure 2h,i show the thermal degradation behavior of GO, ChNCs, D-ChNCs, and D-ChNCs/GO. All the samples begin to lose weight below 100 °C because of moisture loss. A sharp weight loss of the GO nanosheets appears at 190−243 °C as a result of chemical decomposition of the oxygenated functional groups.[33] The maximum decomposition temperature of D-ChNCs increases to 383 from 343 °C of ChNCs, suggesting that the surface-grafted PDA layer could improve the thermal stability of ChNCs. D-ChNCs/GO exhibits two maximum decomposition peak temperatures of 191 and 368 °C, which is consistence with the characteristic degradation peaks of GO and D-ChNCs.

To further study the chemical structure, the XPS spectra of GO and D-ChNCs/GO were characterized (Figure 3). The peaks in the spectrum of GO at around 285 and 535 eV correspond to the 1s orbital electrons of carbon and oxygen, respectively (Figure 3a). However, an increased N 1s peak at around 402 eV is found in the spectrum of D-ChNCs/GO (Figure 3c). The C 1s peak of GO can be divided into four peaks at 284.5 eV (C−C), 286.6 eV (C−O), 287.2 eV (C═O), and 288.4 eV (O−C═O) (Figure 3b).[34] However, the C 1s peak of D-ChNCs/GO can be divided into five peaks at 284.6, 285.4, 286.6, 287.2, and 288.4 eV, corresponding to C−C, C−N, C−O, C═O, and O−C═O bands, respectively (Figure 3d). For the D-ChNCs/GO sample, the new peak of C−N is attributed to the −NHCO− functional groups in the ChNC chains and a PDA layer rich in amine groups and imine groups.[35,36] The elemental composition of GO (the inset table in Figure 3a) is C (64.92%) and O (33.40%), while the elemental composition of D-ChNCs/GO (the inset table in Figure 3c) is C (53.23%), O (31.25%), and N (15.52%). The XPS result of the composite membrane further demonstrates the presence of ChNCs in the layer structure of GO membrane.

The morphology of ChNCs, D-ChNCs, and D-ChNCs/GO was characterized by TEM (Figure 4). The morphology of ChNCs shows a uniform needlelike nanostructure with a length and a width range of 100−500 and 15−30 nm, respectively (Figure 4a,b). ChNCs exhibit a high aspect ratio of 3−15. As a result of electrostatic repulsion between the positively charged chitin molecules, ChNCs are evenly distributed in aqueous suspension after ultrasonication treatment.[37] The outer surfaces of ChNCs are uniformly covered with black PDA particles via polymerization reaction (Figure 4c,d), illustrating the successful synthesis of D-ChNCs. Meanwhile, D-ChNCs display some aggregates as ChNCs can be cross-linked by PDA. As displayed in Figure 4e,f, GO is structured with two-dimensional nanoscale sheets stacking with strong $\pi-\pi$ band.[38] The images also reveal the presence of large GO sheets adhered to needlelike D-ChNCs via hydrogen bond interaction among the surface hydroxyl groups

DOI: 10.1021/acssuschemeng.9b02619
ACS Sustainable Chem. Eng. 2019, 7, 13379−13390

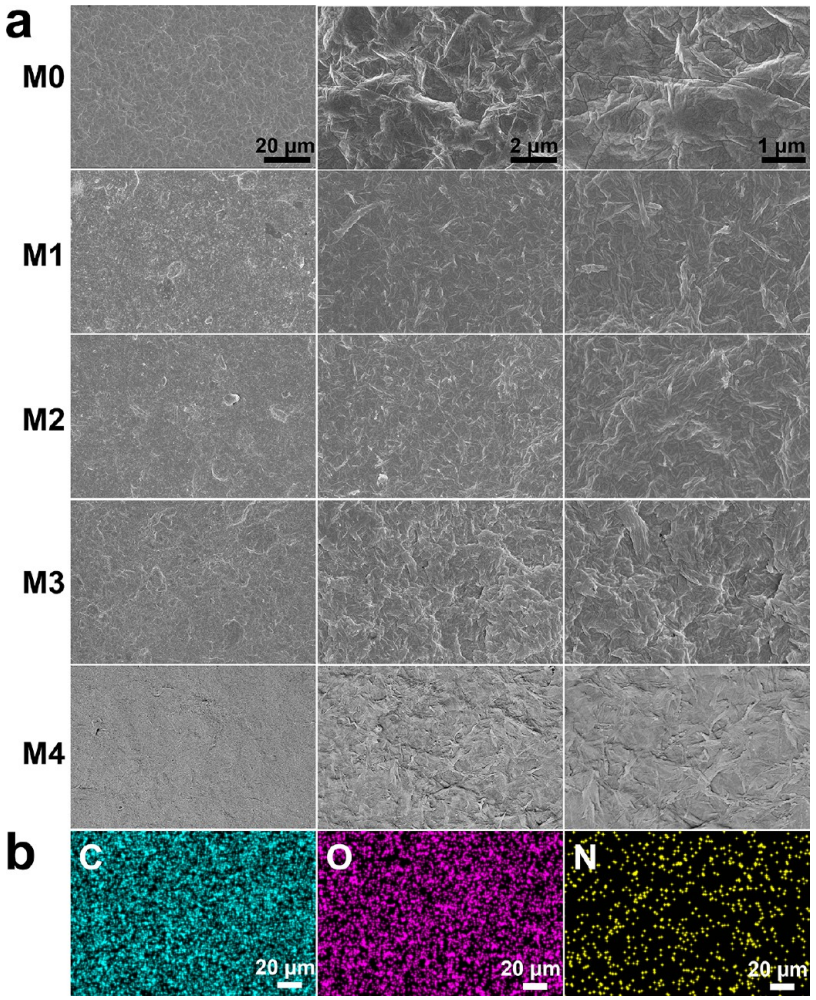

Figure 5. SEM images of different membranes (a); EDS elemental mapping of M4 surface (b).

of GO and D-ChNCs,[39] which indicates the successful combination of D-ChNCs and GO nanosheets. Combinations with the different morphologies of D-ChNCs and GO nanosheets are beneficial to the formation of hierarchical nanostructures to selectively transport water molecule and ions.[40]

The surface morphologies of GO and composite membranes are shown in Figure 5a. M0 sample is stacked by GO nanosheets layer-by-layer, showing a smooth and neat surface with wrinkled corrugations. In case of the composite membranes, rigid D-ChNCs are observed to evenly embed in the interlayer of GO nanosheets. The surface morphology of composite membranes is rougher and the stacked wrinkles of GO are overlapped by nanorods with the enhancing intercalation of D-ChNCs. The composite membrane is nearly dense without visible pore. This result is also consistent with the roughness measurement of 3D AFM above. The intercalation of D-ChNCs could rationally control the layered structures of GO and provide a tunable nanochannel structure for water molecules flux. The elemental distribution of C, O, and N on the surface of M4 is displayed in EDS elemental mapping (Figure 5b). The N element is derived from ChNCs and PDA. C, O, and N elements are well-distributed on the surface of composite membrane, which demonstrates that ingredients are uniformly dispersed and interpenetrated forming 3D nanostructure.

As a supporting membrane, the physicochemical properties and surface morphology of CAM is significant for D-ChNCs/GO membrane in the application of dye and oil separation. IR and XRD spectra, SEM, and water contact angle of CAM analyses have been carried out. As shown as in Figure S1a, the adsorption bands of base membrane are at 3490 cm^{-1} (O−H shrinking vibration), 1695 cm^{-1} (C═O stretching), and 900 cm^{-1} (C−O vibration), respectively.[41,42] A broad peak at 21.3° in XRD pattern (Figure S1b) corresponds to the cellulose acetate matrix.[43] It can be observed from SEM (Figure S1c) that the base membrane exhibits porous structure with the pore size of 0.44−2.20 μm. Furthermore, the base membrane has a water contact angle of 66.0° ± 2.8 (Figure S1d).

Contact Angle and Pure Water Flux. To evaluate the wettability of membranes, both contact angle and pure water flux were measured (Figure 6). With the increasing content of D-ChNCs in GO membrane, the water contact angles gradually decrease from 58.7 to 44.9°, indicating a better hydrophilicity of the composite membrane. A higher hydrophilicity of D-ChNCs/GO membrane contributes to plentiful hydrophilic groups derived from surface ChNC molecular chains (hydroxyl, *N*-acetyl, and amino groups) and PDA (phenolic hydroxyl groups and imino groups).[36] A large number of hydrophilic groups could enhance the ability of hydration on the composite membrane surface.[15] The result of contact angle is also corresponded with pure water flux. The

DOI: 10.1021/acssuschemeng.9b02619
ACS Sustainable Chem. Eng. 2019, 7, 13379−13390

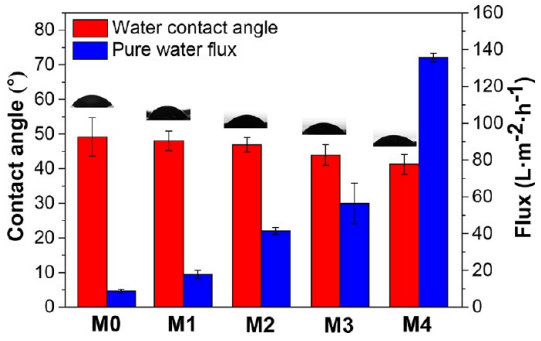

Figure 6. Contact angle and pure water flux of different membranes.

pure water flux of membrane dramatically increases from 8.8 L·m^{-2}·h^{-1} for M0 to 135.6 L·m^{-2}·h^{-1} for M4. The uniform intercalation of needlelike D-ChNCs enhances the interlayer distance of adjacent GO sheets, forming a nanochannel structure for water molecules. In addition, high wettability could facilitate the interaction with water and membrane interfaces due to plenty of hydrophilic groups on the membranes. Therefore, different contents of D-ChNCs could be effective to manipulate the tunnel structure of GO via the vacuum filtration method.

Dyes Removal Experiments. MB and CR were selected as a model of cationic and anionic dye-contaminated wastewater, respectively. As displayed in Figure 7a,d, the rejection ratio of MB and CR on the CAM is 12.3 and 8.7%, respectively. In contrast, the removal efficiency of dye is highly enhanced upon the introduction of GO and D-ChNCs. It is clear that the rejection ratios of MB are all above 98.0% on the composite membranes (M0 (99.8%), M1 (98.0%), M2 (99.6%), M3 (99.9%), and M4 (99.3%)), while the rejection ratios of CR on the M0, M1, M2, M3, and M4 are 89.5, 98.2, 98.3, 95.0, and 97.8%, respectively. This result is also consistent with UV−vis absorption experiments result of permeated solution (Figure 7c,f). Compared with the sample of feed solution, no absorption peak can be identified in the wavelength of 664 nm (MB) and 488 nm (CR) on the M0, M1, M2, M3, and M4. However, the dye solution samples after filtration on the CAM show much higher absorbance. Moreover, the permeated solution of MB and CR after filtration on the composite membrane displays transparent in inset photographs after permeation. The separation efficiency of MB and CR is then evaluated by dye flux (Figure 7b,e). Due

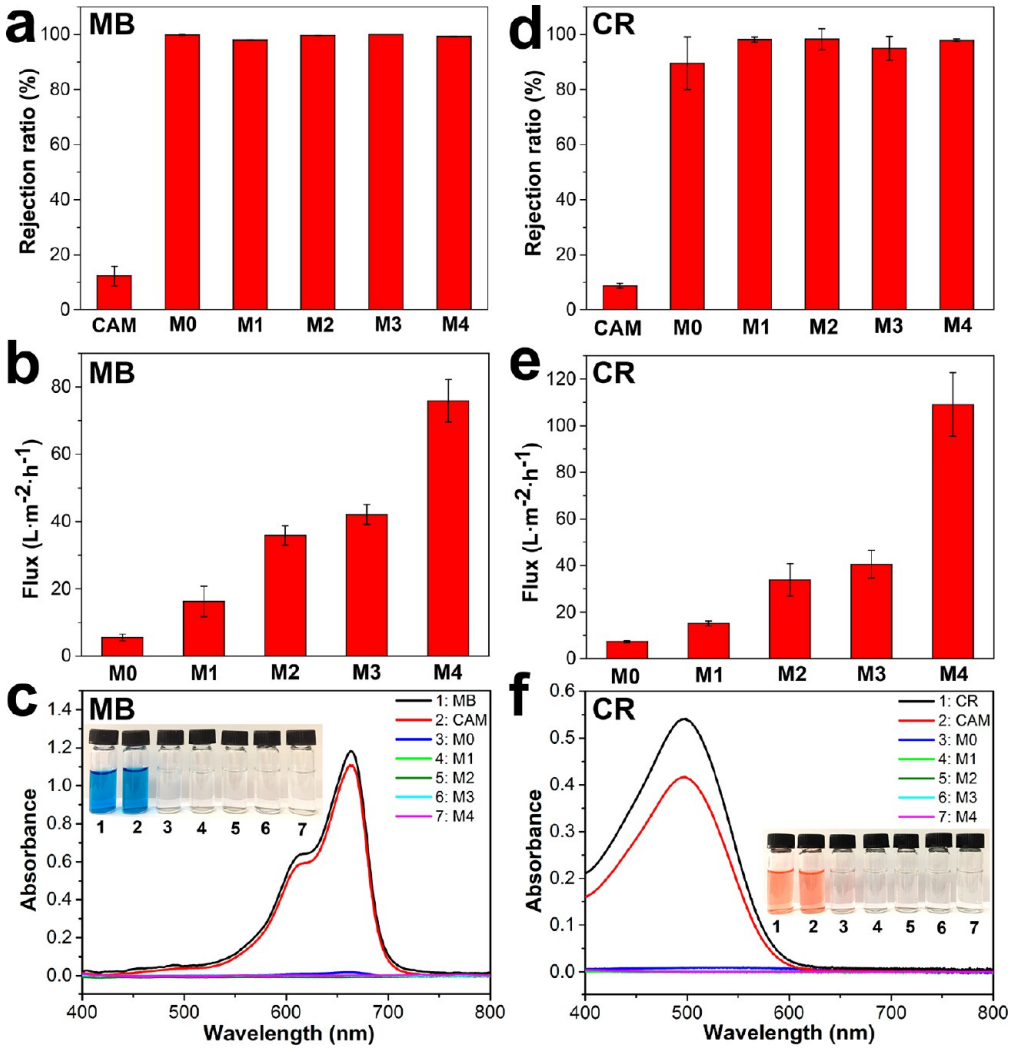

Figure 7. Dye removal performance of different composite membranes: MB (a) and CR (d) rejection ratio; MB (b) and CR (e) flux; UV−vis absorption experiments of MB (c) and CR (f).

DOI: 10.1021/acssuschemeng.9b02619
ACS Sustainable Chem. Eng. 2019, 7, 13379−13390

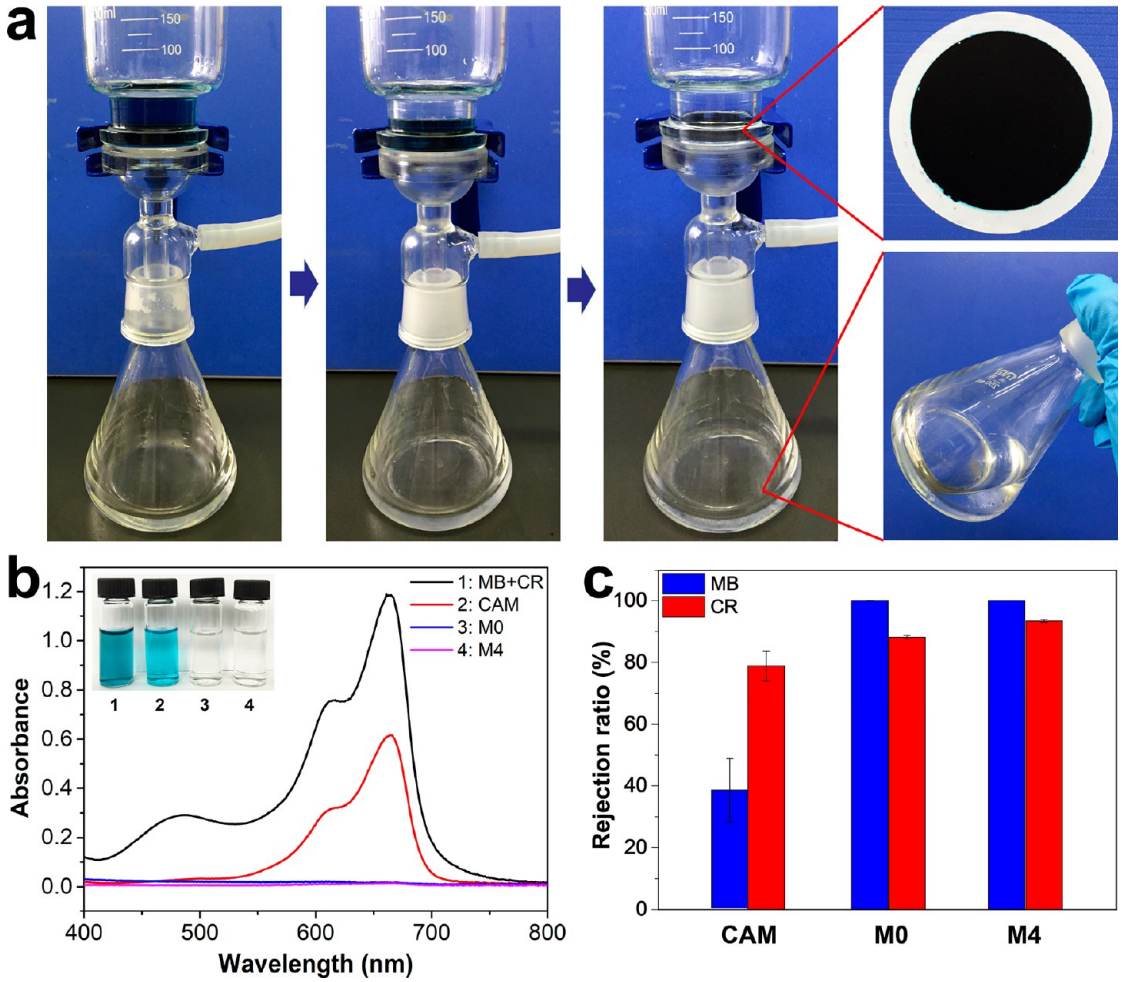

Figure 8. Separation process of MB and CR mixture (50% v/v) (a); UV−vis absorption experiment of the dye mixture (b); MB and CR rejection ratio of CAM, M0, and M4 (c).

to the oxygen-containing functional groups, GO surface with negative charge could be effective in adsorbing positively charged organic molecules (MB).[44] Meanwhile, ChNCs with positive charge due to protonated amino groups could interact with anionic dye (CR).[45] Besides, PDA with catechol groups and ethylamino groups could facilitate the adsorption of MB and CR. It is reported that GO and ChNCs with high surface area also play a major part in separation behavior.[46,47] The dye flux of M0 for MB and CR is extremely poor, which is attributed to that the tightly packed GO nanosheets block the transport of water molecules. Upon the incorporation of D-ChNCs, the dye flux gradually increases from 5.5 to 75.9 L·m^{-2}·h^{-1} (MB) and 7.2 to 109.2 L·m^{-2}·h^{-1} (CR). These results suggest that a pathway architecture in the D-ChNCs/GO composite membrane contributes to higher dye flux. The dye fluxes in Figure 7 are lower than the pure water fluxes shown in Figure 6. This can be understood by the dye molecules being stackable on the surfaces of the membrane during the filtration process, which possibly blockes some of the holes for water molecules. This also resultes in concentration polarization that increases filtration obstruction.[40]

To further evaluate the removal performance, the separation experiment of a mixture of dyes (MB and CR, 50% v/v) was carried out on the M4 (Figure 8). The separation process of MB and CR mixture is shown in Figure 8a. It is obvious that the collected permeation dye solution is clear and transparent. As shown in the inset photograph in Figure 8a, MB and CR molecules are absorbed by an as-prepared composite membrane via construction of a hierarchical structure of GO sheets intercalated by D-ChNCs. There is no absorption peak emerging at the wavelengths of 664 nm for MB and 488 nm for CR in the samples of M0 and M4, whereas the CAM exhibits weak adsorption effect toward MB (Figure 8b). The rejection ratio of MB and CR on the M4 is much higher than that of M0, which is due to the interaction with intercalated D-ChNCs and organic dye molecules (Figure 8c). Especially, the MB and CR rejection ratios of CAM could reach 38.1 and 78.6%, which is much higher than that in the separation of MB and CR adsorption experiments above. The dye deposition is formed due to the electrostatic attraction with cationic MB and anionic CR, which advances the capacity of dye separation of the membrane.[48] The dye adsorption behavior analysis has been done at salt concentration of 10 g/L (Figure S2). It is found that the rejection ratio of dye in the presence of NaCl is as high as that of pure dye. However, the flux slightly decreases compared to that of pure dye, as a result of the obstruction of salt ions for water molecules during the filtration. However, the dyes could be also effectively separated from salt solution with high rejection. It is reported that a high or low pH induces a slightly lowered permeated flux as a result of changes in the chemico-physical structures of GO nanosheets.[15] In contrast, elevated temperature increases dye adsorption capacity due to

DOI: 10.1021/acssuschemeng.9b02619
ACS Sustainable Chem. Eng. 2019, 7, 13379−13390

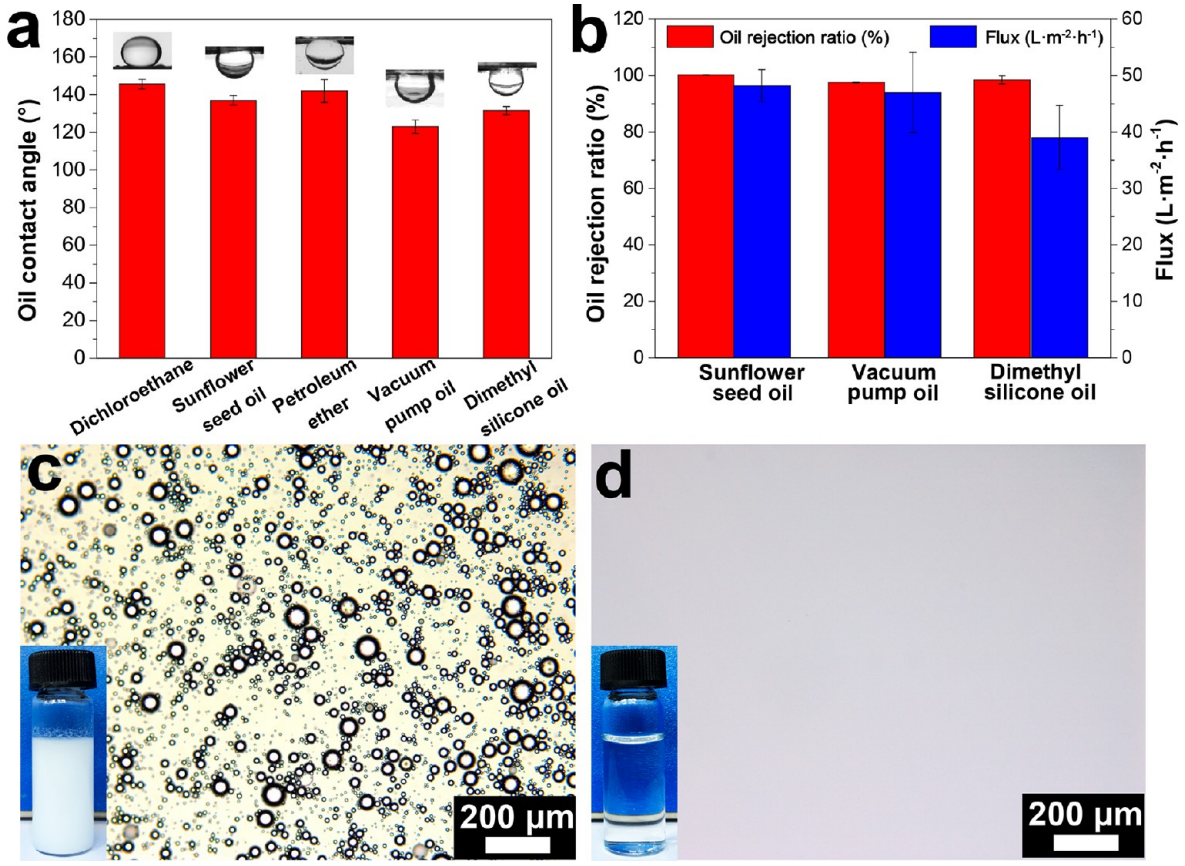

Figure 9. Underwater-oil contact angle (a) and oil rejection and flux (b) of M4; microscope photographs of oil/water mixture before (c) and after (d) filtration.

the enhancement of binding interactions between the dyes and membranes, and the dye adsorption process is an endothermic and spontaneous process.[40]

Oil/Water Separation. As shown in Figure 9a, the underwater−oil contact angle of M4 is measured as 145.7° (dichloroethane), 137.0° (sunflower seed oil), 142.1° (petroleum ether), 123.0° (vacuum pump oil), and 131.5° (dimethyl silicone oil). The underwater−oil droplets on the membrane were also photographed. The underwater−oil contact angle over 90° shows the good oleophobicity of composite membrane. Two factors affect underwater−oil contact angle. On one hand, the coarse nanostructure of membrane surface is major factor of oleophobic property. It is reported that a higher surface roughness could facilitate oil-repellency for membranes.[49] On the other hand, the formation of hydration structure can hinder the oil droplets from contacting with the surface of membrane.[15] The oil rejection ratios and fluxes were characterized in Figure 9b. The rejection ratios of different oil are all above 97.5% on the M4, showing the excellent oil separation of as-prepared membranes. Moreover, the oil flux reaches above 39.0 $L{\cdot}m^{-2}{\cdot}h^{-1}$, which is lower than the flux of dye removal. This result clearly attributes that the passageways on the membrane are partly blocked by the accumulation of oil droplets, which affects the permeation of water molecules. The microscopy photographs of oil/water mixture before and after filtration are displayed in Figure 9c,d. The feed solution exhibits a milk-white turbid state and the oil droplets are well-dispersed by surfactant. In contrast, the filtrated solution is absolutely clear and there is no oil droplet observed in microscopy image. All the results indicate that composite membrane exhibits good oleophobicity and excellent oil/water separation performance.

Recyclable and Antifouling Performance of Membrane. The proper recyclability of membrane is a significant factor for practical application. The CR and sunflower seed oil in water solution were used to evaluate the recyclable and antifouling performance. The membrane was first washed using absolute ethanol and ultrapure water after being fouled each time. As shown in Figure 10a, with an increase in the number of cycles, the rejection ratio for oil in water solution declines a bit, but it is still higher than 97.2% after 5 cycles. The separation efficiency of CR retains 96.4% after 4 cycles, but it gradually drops down to 91.6% after 5 cycles. Meanwhile, the anti-dye- and anti-oil-fouling processes are displayed in Figure 10b,c. The recyclability and antifouling property of membrane involves a synergistic effect of internal laminated structure, electrostatic interaction, and surface functional groups. Therefore, it is believed that D-ChNCs/GO membrane could have acceptable reusability and proper regeneration for practical application due to its special interlayered structure and surface chemical composition.

Comparison with Other Materials. The separation efficiency and permeated flux of several materials are compared in Figure 11. The rejection ratio of all kinds of membranes can reach over 95.3%, but the permeated flux varies different kinds of membranes. The membranes of calcium alginate/sodium alginate (CaAlg/NaAlg),[50] polyamide/graphene oxide (PA/GO),[51] and deoxygenated graphene oxide (DGO)[52] show high rejection ratios, but they exhibit much lower permeated fluxes which may restrict their actual application in wastewater

DOI: 10.1021/acssuschemeng.9b02619
ACS Sustainable Chem. Eng. 2019, 7, 13379−13390

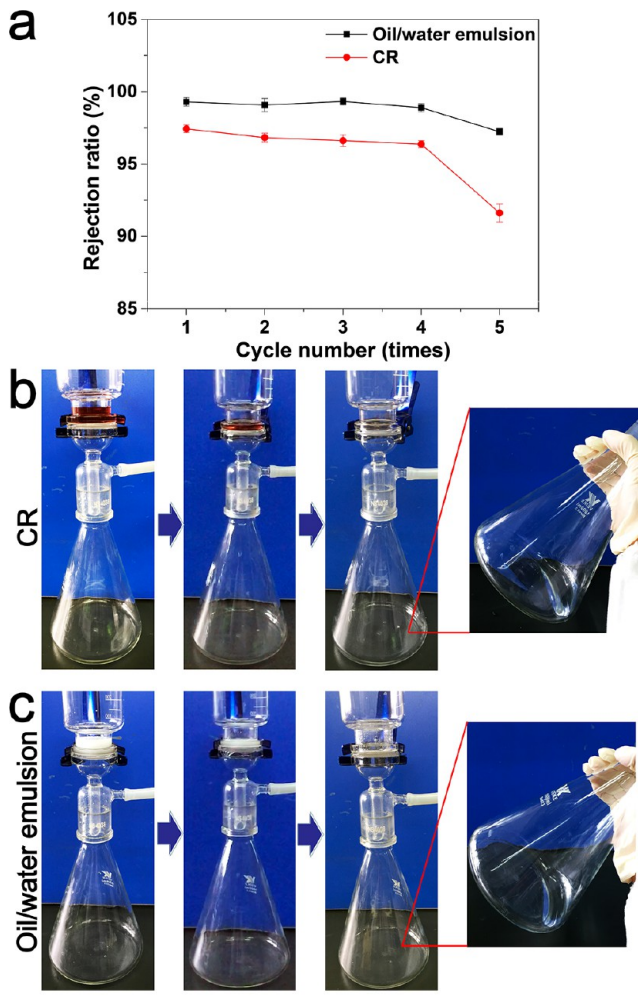

Figure 10. Dye and oil/water separation efficiency versus the recycle numbers by taking CR solution and sunflower seed oil/water emulsion as an example (a); the removal processes of CR solution (b) and oil/water emulsion (c).

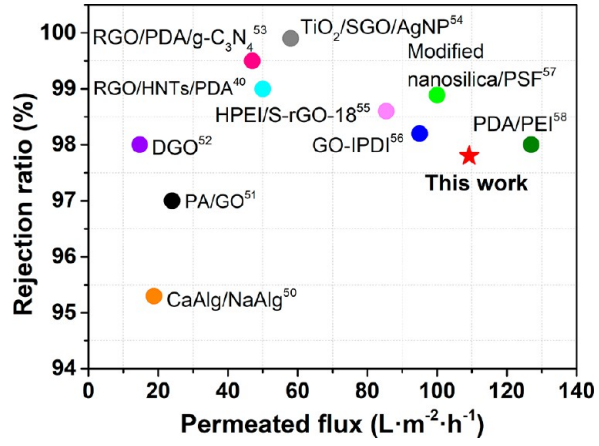

Figure 11. Separation performance of other kinds of researched membranes.

treatment. The membranes of reduced graphene oxide/halloysite nanotubes/polydopamine (RGO/HNTs/PDA),[40] reduced graphene oxide/graphitic carbon nitride sheet membrane (RGO/PDA/g-C_3N_4),[53] and TiO_2/sulfonated graphene oxide/Ag nanoparticle (TiO_2/SGO/AgNP)[54] possess excellent rejection ratios of above 99.0% but with moderate permeated fluxes. Particularly, the other membranes show not only high rejection ratios but also high permeated fluxes including hyperbranched polyethylenimine/solvated reduced graphene oxide (HPEI/S-rGO-18),[55] graphene-isophorone diisocyanate (GO-IPDI),[56] modified nanosilica/polysulfone (PSF),[57] and polydopamine/polyethylenimine (PDA/PEI).[58] The prepared D-ChNCs/GO membrane in the present work also possesses a high rejection ratio (97.8%) and a high permeated flux (109.2 $L{\cdot}m^{-2}{\cdot}h^{-1}$). The separation performance of D-ChNCs/GO membrane is comparable with PDA/PEI composite. In summary, the D-ChNCs/GO composite membrane exhibits proper permeated flux, high rejection ratios of dye and oil/water solution, and good regeneration performance. Therefore, this membrane is believed to be a promising material in wastewater treatment.

CONCLUSION

A free-standing D-ChNCs/GO composite membrane was successfully prepared via a vacuum filtration self-assembly method. Needlelike D-ChNCs are evenly intercalated into interlayered GO nanosheets, greatly enhancing the distance of GO layer. The tunable channel structure of ChNCs and the surface modification by PDA synergistically facilitate surface hydrophilicity, water permeability, and dye and oil/water solution separation efficiency. The pure water flux of M4 is 135.6 $L{\cdot}m^{-2}{\cdot}h^{-1}$, whereas that of M0 is only 8.8 $L{\cdot}m^{-2}{\cdot}h^{-1}$. The dyes rejection ratio of M4 could reach as high as 99.3% for MB and 97.8% for CR. D-ChNCs/GO composite membrane exhibits good oleophobicity with an oil rejection ratio of above 97.5%. Meanwhile, this membrane exhibits acceptable recyclability and proper regeneration for practical application with its special water transport pathways structure. All these results indicate that the D-ChNCs/GO composite membrane has potential applications in wastewater treatment.

ASSOCIATED CONTENT

Supporting Information

The Supporting Information is available free of charge on the ACS Publications website at DOI: 10.1021/acssuschemeng.9b02619.

IR and XRD spectra, SEM, and water contact angle of CAM; rejection ratios and fluxes of pure and salt-containing dye solutions (PDF)

AUTHOR INFORMATION

Corresponding Author

*E-mail: liumx@jnu.edu.cn.

ORCID

Mingxian Liu: 0000-0002-5466-3024

Notes

The authors declare no competing financial interest.

ACKNOWLEDGMENTS

This work was financially supported by the National Natural Science Foundation of China (51473069 and 51502113), the Pearl River S&T Nova Program of Guangzhou (201610010026), and the Fundamental Research Funds for the Central Universities (21619102).

DOI: 10.1021/acssuschemeng.9b02619
ACS Sustainable Chem. Eng. 2019, 7, 13379−13390

REFERENCES

(1) Gao, C.; Sun, Z.; Li, K.; Chen, Y.; Cao, Y.; Zhang, S.; Feng, L. Integrated Oil Separation and Water Purification by a Double-Layer TiO_2-Based Mesh. *Energy Environ. Sci.* **2013**, *6* (4), 1147−1151.

(2) Kurniawan, T. A.; Sillanpää, M. E. T.; Sillanpää, M. Nanoadsorbents for Remediation of Aquatic Environment: Local and Practical Solutions for Global Water Pollution Problems. *Crit. Rev. Environ. Sci. Technol.* **2012**, *42* (12), 1233−1295.

(3) Song, K.; Xu, H.; Xu, L.; Xie, K.; Yang, Y. Cellulose Nanocrystal-Reinforced Keratin Bioadsorbent for Effective Removal of Dyes from Aqueous Solution. *Bioresour. Technol.* **2017**, *232*, 254−262.

(4) Zeng, G.; He, Y.; Zhan, Y.; Zhang, L.; Pan, Y.; Zhang, C.; Yu, Z. Novel Polyvinylidene Fluoride Nanofiltration Membrane Blended with Functionalized Halloysite Nanotubes for Dye and Heavy Metal Ions Removal. *J. Hazard. Mater.* **2016**, *317* (5), 60−72.

(5) Sun, H.; Cao, L.; Lu, L. In Magnetite/Reduced Graphene Oxide Nanocomposites: One Step Solvothermal Synthesis and Use as a Novel Platform for Removal of Dye Pollutants. *Nano Res.* **2011**, *4* (6), 550−562.

(6) Vasilios, G.; Michal, O.; Bourlinos, A. B.; Vimlesh, C.; Namdong, K.; K Christian, K.; Pavel, H.; Radek, Z.; Kim, K. S. Functionalization of Graphene: Covalent and Non-Covalent Approaches, Derivatives and Applications. *Chem. Rev.* **2012**, *112* (11), 6156−6214.

(7) Zhu, Y.; Murali, S.; Cai, W.; Li, X.; Suk, J. W.; Potts, J. R.; Ruoff, R. S. Graphene and Graphene Oxide: Synthesis, Properties, and Applications. *Adv. Mater.* **2010**, *22* (35), 3906−3924.

(8) Wang, K.; Ruan, J.; Song, H.; Zhang, J.; Wo, Y.; Guo, S.; Cui, D. Biocompatibility of Graphene Oxide. *Nanoscale Res. Lett.* **2011**, *6* (1), 8.

(9) Li, J.; Kuang, D.; Feng, Y.; Zhang, F.; Xu, Z.; Liu, M. A Graphene Oxide-Based Electrochemical Sensor for Sensitive Determination of 4-Nitrophenol. *J. Hazard. Mater.* **2012**, *201* (1), 250−259.

(10) Wang, L.; Lee, K.; Sun, Y. Y.; Lucking, M.; Chen, Z.; Zhao, J. J.; Zhang, S. B. Graphene Oxide as an Ideal Substrate for Hydrogen Storage. *ACS Nano* **2009**, *3* (10), 2995−3000.

(11) Min, S. K.; Kim, W. Y.; Cho, Y.; Kim, K. S. Fast DNA Sequencing with a Graphene-Based Nanochannel Device. *Nat. Nanotechnol.* **2011**, *6* (3), 162−165.

(12) Smith, Z. P.; Freeman, B. D. Graphene Oxide: A New Platform for High-Performance Gas- and Liquid-Separation Membranes. *Angew. Chem., Int. Ed.* **2014**, *53* (39), 10286−10288.

(13) Ramesha, G.K.; Vijaya Kumara, A.; Muralidhara, H.B.; Sampath, S. Graphene and Graphene Oxide as Effective Adsorbents toward Anionic and Cationic Dyes. *J. Colloid Interface Sci.* **2011**, *361* (1), 270−277.

(14) Compton, O. C.; Nguyen, S. B. T. Graphene Oxide, Highly Reduced Graphene Oxide, and Graphene: Versatile Building Blocks for Carbon-Based Materials. *Small* **2010**, *6* (6), 711−723.

(15) Zhao, X.; Su, Y.; Liu, Y.; Li, Y.; Jiang, Z. Free-Standing Graphene Oxide-Palygorskite Nanohybrid Membrane for Oil/Water Separation. *ACS Appl. Mater. Interfaces* **2016**, *8* (12), 8247−8256.

(16) Zeng, G.; He, Y.; Ye, Z.; Yang, X.; Chen, X.; Ma, J.; Li, F. Novel Halloysite Nanotubes Intercalated Graphene Oxide-Based Composite Membranes for Multifunctional Applications: Oil/Water Separation and Dyes Removal. *Ind. Eng. Chem. Res.* **2017**, *56* (37), 10472−10481.

(17) Han, Y.; Jiang, Y.; Gao, C. High-Flux Graphene Oxide Nanofiltration Membrane Intercalated by Carbon Nanotubes. *ACS Appl. Mater. Interfaces* **2015**, *7* (15), 8147−8155.

(18) Kumar, M. N. V. R. Chitin and Chitosan Fibres: A Review. *Bull. Mater. Sci.* **1999**, *22* (5), 905−915.

(19) Zeng, J. B.; He, Y. S.; Li, S. L.; Wang, Y. Z. Chitin Whiskers: An Overview. *Biomacromolecules* **2012**, *13* (1), 1−11.

(20) Wongpanit, P.; Sanchavanakit, N.; Pavasant, P.; Bunaprasert, T.; Tabata, Y.; Rujiravanit, R. Preparation and Characterization of Chitin Whisker-Reinforced Silk Fibroin Nanocomposite Sponges. *Eur. Polym. J.* **2007**, *43* (10), 4123−4135.

(21) Ma, B.; Qin, A.; Li, X.; Zhao, X.; He, C. Structure and Properties of Chitin Whisker Reinforced Chitosan Membranes. *Int. J. Biol. Macromol.* **2014**, *64* (2), 341−346.

(22) Zhan, H.; Zuo, T.; Tao, R.; Chang, C. Robust Tunicate Cellulose Nanocrystal/Palygorskite Nanorod Membranes for Multifunctional Oil/Water Emulsion Separation. *ACS Sustainable Chem. Eng.* **2018**, *6* (8), 10833−10840.

(23) Cheng, Q.; Ye, D.; Chang, C.; Zhang, L. Facile Fabrication of Superhydrophilic Membranes Consisted of Fibrous Tunicate Cellulose Nanocrystals for Highly Efficient Oil/Water Separation. *J. Membr. Sci.* **2017**, *525*, 1−8.

(24) Ma, H.; Wang, S.; Meng, F.; Xu, X.; Huo, X. A Hydrazone-Carboxyl Ligand-Linked Cellulose Nanocrystal Aerogel with High Elasticity and Fast Oil/Water Separation. *Cellulose* **2017**, *24* (2), 797−809.

(25) Nair, K. G.; Dufresne, A. Crab Shell Chitin Whisker Reinforced Natural Rubbernanocomposites. 1. Processing and Swelling Behavior. *Biomacromolecules* **2003**, *4* (3), 657−665.

(26) Zhong, Z.; Xing, W.; Zhang, B. Fabrication of Ceramic Membranes with Controllable Surface Roughness and Their Applications in Oil/Water Separation. *Ceram. Int.* **2013**, *39* (4), 4355−4361.

(27) Guo, H.; Peng, M.; Zhu, Z.; Sun, L. Preparation of Reduced Graphene Oxide by Infrared Irradiation Induced Photothermal Reduction. *Nanoscale* **2013**, *5* (19), 9040−9048.

(28) Zhao, C.; Xu, X.; Chen, J.; Yang, F. Effect of Graphene Oxide Concentration on the Morphologies and Antifouling Properties of PVDF Ultrafiltration Membranes. *J. Environ. Chem. Eng.* **2013**, *1* (3), 349−354.

(29) Ifuku, S.; Nogi, M.; Abe, K.; Yoshioka, M.; Morimoto, M.; Saimoto, H.; Yano, H. Preparation of Chitin Nanofibers with a Uniform Width as α-Chitin from Crab Shells. *Biomacromolecules* **2009**, *10* (6), 1584−1588.

(30) Yang, K.; Lee, J. S.; Kim, J.; Lee, Y. B.; Shin, H.; Um, S. H.; Kim, J. B.; Park, K. I.; Lee, H.; Cho, S.-W. Polydopamine-Mediated Surface Modification of Scaffold Materials for Human Neural Stem Cell Engineering. *Biomaterials* **2012**, *33* (29), 6952−6964.

(31) Rani, S.; Kumar, M.; Kumar, R.; Kumar, D.; Sharma, S.; Singh, G. Characterization and Dispersibility of Improved Thermally Stable Amide Functionalized Graphene Oxide. *Mater. Res. Bull.* **2014**, *60*, 143−149.

(32) Huang, Y.; Yao, M.; Zheng, X.; Liang, X.; Su, X.; Zhang, Y.; Lu, A.; Zhang, L. Effects of Chitin Whiskers on Physical Properties and Osteoblast Culture of Alginate Based Nanocomposite Hydrogels. *Biomacromolecules* **2015**, *16* (11), 3499−3507.

(33) Zeng, Y.; Zhou, Y.; Kong, L.; Zhou, T.; Shi, G. A Novel Composite of SiO_2-Coated Graphene Oxide and Molecularly Imprinted Polymers for Electrochemical Sensing Dopamine. *Biosens. Bioelectron.* **2013**, *45* (1), 25−33.

(34) Xu, L. Q.; Yang, W. J.; Neoh, K.-G.; Kang, E.-T.; Fu, G. D. Dopamine-Induced Reduction and Functionalization of Graphene Oxide Nanosheets. *Macromolecules* **2010**, *43* (20), 8336−8339.

(35) Li, H. Y.; Li, H.; Wang, B. J.; Gu, Q.; Jiang, Z. Q.; Wu, X. D. Synthesis and Properties of Poly(3-Hydroxybutyrate-Co-3-Hydroxyvalerate)/Chitin Nanocrystals Composite Scaffolds for Tissue Engineering. *Chin. Chem. Lett.* **2014**, *25* (12), 1635−1638.

(36) Zhu, L.; Lu, Y.; Wang, Y.; Zhang, L.; Wang, W. Preparation and Characterization of Dopamine-Decorated Hydrophilic Carbon Black. *Appl. Surf. Sci.* **2012**, *258* (14), 5387−5393.

(37) Lin, N.; Zhao, S.; Gan, L.; Chang, P. R.; Xia, T.; Huang, J. Preparation of Fungus-Derived Chitin Nanocrystals and Their Dispersion Stability Evaluation in Aqueous Media. *Carbohydr. Polym.* **2017**, *173*, 610−618.

(38) Li, Z.; Liu, Z.; Sun, H.; Gao, C. Superstructured Assembly of Nanocarbons: Fullerenes, Nanotubes, and Graphene. *Chem. Rev.* **2015**, *115* (15), 7046−7117.

(39) Wang, R.; Li, Z.; Liu, W.; Jiao, W.; Hao, L.; Yang, F. Attapulgite−Graphene Oxide Hybrids as Thermal and Mechanical

DOI: 10.1021/acssuschemeng.9b02619
ACS Sustainable Chem. Eng. 2019, 7, 13379−13390

Reinforcements for Epoxy Composites. *Compos. Sci. Technol.* **2013**, *87* (9), 29−35.
(40) Liu, Y.; Tu, W.; Chen, M.; Ma, L.; Yang, B.; Liang, Q.; Chen, Y. A Mussel-Induced Method to Fabricate Reduced Graphene Oxide/Halloysite Nanotubes Membranes for Multifunctional Applications in Water Purification and Oil/Water Separation. *Chem. Eng. J.* **2018**, *336*, 263−277.
(41) Ryu, J. H.; Lee, H.; Kim, Y. J.; Kang, Y. S.; Kim, H. S. Facilitated Olefin Transport by Reversible Olefin Coordination to Silver Ions in a Dry Cellulose Acetate Membrane. *Chem. - Eur. J.* **2001**, *7* (7), 1525−1529.
(42) Skorayakov, I. V.; Komar, V. P. Determination of the Content of Bound Acetic Acid in Cellulose Acetates by the Method of IR Spectroscopy. *J. Appl. Spectrosc.* **1994**, *61* (3−4), 558−563.
(43) Chaurasia, V.; Chand, N.; Bajpai, S. K. Water Sorption Properties and Antimicrobial Action of Zinc Oxide Nanoparticles-Loaded Cellulose Acetate Films. *J. Macromol. Sci., Chem.* **2010**, *47* (4), 309−317.
(44) Wang, L.; Xin, X.; Yang, M.; Ma, X.; Shen, J.; Song, Z.; Yuan, S. Effects of Graphene Oxide and Salinity on Sodium Deoxycholate Hydrogels and Their Applications in Dye Absorption. *Colloid. Surface A* **2015**, *483*, 112−120.
(45) Revol, J. F.; Marchessault, R. H. In Vitro Chiral Nematic Ordering of Chitin Crystallites. *Int. J. Biol. Macromol.* **1993**, *15* (6), 329−335.
(46) Dong, Z.; Wang, D.; Liu, X.; Pei, X.; Chen, L.; Jin, J. Bio-Inspired Surface-Functionalization of Graphene Oxide for the Adsorption of Organic Dyes and Heavy Metal Ions with a Superhigh Capacity. *J. Mater. Chem. A* **2014**, *2* (14), 5034−5040.
(47) Goodrich, J. D.; Winter, W. T. α-Chitin Nanocrystals Prepared from Shrimp Shells and Their Specific Surface Area Measurement. *Biomacromolecules* **2007**, *8* (1), 252−257.
(48) Yang, G.; Wu, L.; Xian, Q.; Shen, F.; Wu, J.; Zhang, Y. Removal of Congo Red and Methylene Blue from Aqueous Solutions by Vermicompost-Derived Biochars. *PLoS One* **2016**, *11* (5), e0154562.
(49) Hsieh, C. T.; Chen, J. M.; Kuo, R. R.; Lin, T. S.; Wu, C. F. Influence of Surface Roughness on Water- and Oil-Repellent Surfaces Coated with Nanoparticles. *Appl. Surf. Sci.* **2005**, *240* (1), 318−326.
(50) Zhao, K.; Zhang, X.; Wei, J.; Li, J.; Zhou, X.; Liu, D.; Liu, Z.; Li, J. Calcium Alginate Hydrogel Filtration Membrane with Excellent Anti-Fouling Property and Controlled Separation Performance. *J. Membr. Sci.* **2015**, *492*, 536−546.
(51) Bano, S.; Mahmood, A.; Kim, S. J.; Lee, K. H. Graphene Oxide Modified Polyamide Nanofiltration Membrane with Improved Flux and Antifouling Properties. *J. Mater. Chem. A* **2015**, *3* (5), 2065−2071.
(52) Kim, D. W.; Jang, J.; Kim, I.; Nam, Y. T.; Jung, Y.; Jung, H.-T. Revealing the Role of Oxygen Debris and Functional Groups on the Water Flux and Molecular Separation of Graphene Oxide Membrane: A Combined Experimental and Theoretical Study. *J. Phys. Chem. C* **2018**, *122* (30), 17507−17517.
(53) Li, F.; Yu, Z.; Shi, H.; Yang, Q.; Chen, Q.; Pan, Y.; Zeng, G.; Yan, L. A Mussel-Inspired Method to Fabricate Reduced Graphene Oxide/g-C_3N_4 Composites Membranes for Catalytic Decomposition and Oil-in-Water Emulsion Separation. *Chem. Eng. J.* **2017**, *322*, 33−45.
(54) Qian, D.; Chen, D.; Li, N.; Xu, Q.; Li, H.; He, J.; Lu, J. TiO_2/Sulfonated Graphene Oxide/Ag Nanoparticle Membrane: In Situ Separation and Photodegradation of Oil/Water Emulsions. *J. Membr. Sci.* **2018**, *554*, 16−25.
(55) Huang, L.; Chen, J.; Gao, T.; Zhang, M.; Li, Y.; Dai, L.; Qu, L.; Shi, G. Reduced Graphene Oxide Membranes for Ultrafast Organic Solvent Nanofiltration. *Adv. Mater.* **2016**, *28* (39), 8669−8674.
(56) Zhang, P.; Gong, J. L.; Zeng, G. M.; Deng, C. H.; Yang, H. C.; Liu, H. Y.; Huan, S. Y. Cross-Linking to Prepare Composite Graphene Oxide-Framework Membranes with High-Flux for Dyes and Heavy Metal Ions Removal. *Chem. Eng. J.* **2017**, *322*, 657−666.
(57) Zhang, Y.; Shan, L.; Tu, Z.; Zhang, Y. Preparation and Characterization of Novel Ce-Doped Nonstoichiometric Nanosilica/Polysulfone Composite Membranes. *Sep. Purif. Technol.* **2008**, *63* (1), 207−212.
(58) Yang, H. C.; Liao, K. J.; Huang, H.; Wu, Q. Y.; Wan, L. S.; Xu, Z. K. Mussel-Inspired Modification of a Polymer Membrane for Ultra-High Water Permeability and Oil-in-Water Emulsion Separation. *J. Mater. Chem. A* **2014**, *2* (26), 10225−10230.

DOI: 10.1021/acssuschemeng.9b02619
ACS Sustainable Chem. Eng. 2019, 7, 13379−13390